lubricants

MDPI

Article

Frictional Characteristic Curves of Ground Surfaces in Lubricated Sliding

Gopakumar Parameswaran *, Vikram Jayaram and Satish V. Kailas

Department of Materials Engineering, Indian Institute of Science, Bangalore 560012, Karnataka, India; qjayaram@iisc.ac.in (V.J.); satvk@iisc.ac.in (S.V.K.)
* Correspondence: gopa99@gmail.com

Abstract: The key objective of the presented study was to use a commercially feasible and scalable approach to modifying surfaces to reduce friction. In an industrial setting, surface grinding is commercially viable and scalable as compared to other surface modifying processes like laser surface texturing, plasma, or ion beam milling. Frictional force plots are generated from the lubricated contact interface between a flat-faced aluminum pin and a reciprocating stainless steel countersurface driven by a scotch yoke follower mechanism. Using a surface grinder and selecting coated abrasive sheets, different stainless steel surface specimens, classified as P320, P1200, and mirror were prepared and tested in this study. The frictional force encountered by the pin was recorded using a data acquisition system at discrete intervals in the reciprocating path and averaged along the sliding cycles. The shape of the frictional force plots thus generated were found to be different from each other. Various mechanisms of friction prevalent at the contact were presumed to influence the shape of these frictional plots. These mechanisms were tested by varying the sliding speeds, lubricating oil viscosities, and using tribofilm-forming additives. We used Group 1 base oil of two different viscosities in our tests. At lower speeds, the frictional force plot for the mirror-finished surface seemed to conform to the Stribeck curve, while in the same scale of reference, the P1200 surface had a force plot that was nearly flat and of very low magnitude. At the contact interface, there seemed to be a fine balance existing between adhesion and abrasion phenomena, while oil retention was promoted to achieve extremely low sliding friction.

Keywords: friction; frictional characteristic curves; sliding; surface grinding; random surface texturing; lubrication; topography

Citation: Parameswaran, G.; Jayaram, V.; Kailas, S.V. Frictional Characteristic Curves of Ground Surfaces in Lubricated Sliding. *Lubricants* **2023**, *11*, 354. https://doi.org/10.3390/lubricants11090354

Received: 20 July 2023
Revised: 9 August 2023
Accepted: 19 August 2023
Published: 22 August 2023

1. Introduction

Friction has always been a fundamental criterion for any designer working to improve the efficiency of moving parts and loaded contacts. Early on, history gives us ample evidence of how sliding friction became a prominent subject of study in the Egyptian civilization [1], where heavy structures used in the construction of the pyramids had to be moved around using manual effort. They had realized that introducing animal fats and oils into the sliding interface [2] substantially reduced the effort required to move such heavy loads; this enabled their men to be more productive and these tasks to be carried out faster and more efficiently.

The texturing of surfaces has always caught the attention of designers and scientists alike. Textures available in nature, like the leaves of a lotus flower [3,4] or the wings of a butterfly [5], have always been a matter of popular research, especially after the advent of electron microscopes [6]. A structured surface as defined by Evans et al. [7] is a patterned surface with some regular array of surface height features amenable to some sensible description. Stout et al. [8] defined structured surfaces as those where the surface structure is a design feature intended to give a specific functional performance. Laser surface texturing has been a favorite with researchers [9–12] who intend to study the effect

of surface topography modification on friction. There has been a lot of work done in the past towards understanding the effect of surface topography on sliding friction [12,13]. Conventionally, it is believed that smoother surfaces are always beneficial to sliding as the motion encounters lower hindrances from surface protrusions that would otherwise obstruct the sliding motion. In automotive parlance, the frictional force is considered to "run-in" the mating surfaces and even out the protrusions and make the surfaces level for effective sliding [13,14].

The Stribeck curve and its shapes have been studied by tribologists Schnell et al. [15] while examining their relationship with the surface and the counter surface. Erdemir [16] noted that surface texturing can modify the boundary lubrication regimes by reducing the width and height of the Stribeck curve. In his work, Erdemir could successfully manipulate the classical Stribeck diagrams through laser texturing of a coated surface under boundary-lubricated sliding conditions. The relationship of the film thickness with the Stribeck curve was amply examined by Bayer [17], where both wear and friction are supposed to reduce as the film thickness increases, moving the contact towards the mixed regime of lubrication. Oil film thickness depended on the magnitude of $\eta \cdot N/P$, where η is the oil viscosity, N is the sliding velocity, and P is the normal load; Ludema [18] mentions boundary lubrication as a stage where the oil film thickness becomes comparable to or lower than the height of the surface asperities and metal to metal contact initiates.

Petterson et al. [19,20] in their work on boundary lubrication showed that the mechanism of friction and wear in boundary regime is complex and influenced by surface roughness, surface hardness, lubricants, and wear products. He showed that if the counter surface is soft, the texture could get filled up with wear debris, and if the counter surface is hard, the texture could be worn away. He opined that surfaces that come in intermittent contact are always preferred for texturing as wear particles will not fill the textures as fast; this also helps the surface in reclaiming lubricant from surroundings and increases the longevity of the textures due to lesser wear on the intermittent surface.

Menezes et al. [21,22] proved that random smoother surfaces could retain more oil and hence generate the lowest coefficient of friction during sliding as compared to surfaces prepared by unidirectional grinding. They also found that the adhesive component of friction dominated when the oil film between the sliding interfaces was not retained or was minimal. Wang et al. [23] concluded that the overall frictional force encountered during sliding is the combined effect of adhesive interactions, asperity deformation, and ploughing effects between mating surfaces and is influenced by the lubricant used. Using SEM micrographs on worn surfaces, they showed that wear deformation would be the highest for smooth surfaces as compared to textured surfaces. Maru et al. [24] brought the shortcoming of working with average friction coefficients to classify surfaces on their friction performance into focus.

Though many studies have classified surfaces based on average friction performance during multiple sliding events, not many researchers have tried to analyze and differentiate surfaces using friction as a continuous response. We attempted to classify different surface finishes that are macroscopically similar but microscopically different using their friction response plots. We brought about minor variations in the grit sizes of the abrasive disc and observed its effect on these plots. We discuss the shapes of these frictional force response plots in a sparsely lubricated regime and the effect of different tribo-system parameters on them.

2. Materials and Methods

Stainless steel (Grade 304) flat specimens of Rockwell hardness B98 and a 30 mm square cross-section were laser cut from a single stock of 4 mm thickness; the square faces were ground and polished to mirror-finish using a table grinder fitted with a custom sample holding attachment as shown in Figure 1.

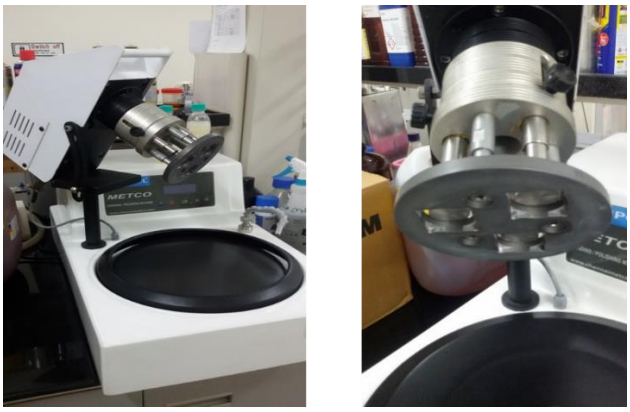

Figure 1. The table grinder with the custom-made square specimen holder.

The mirror-finished specimens were then cleaned ultrasonically using hexane and dried before sandpaper of the select grit was used to grind the surface through a controlled and repeatable process. In this paper, these test specimens are referred to by the grit size of the sandpaper used to render the surface finish; grit sizes are listed according to the "P" scale as per the FEPA standard. Grinding parameters like quantity and flow rate of the coolant, time and speed of grinding, and the contact pressure of the tool were closely monitored and controlled to generate repeatable specimens in this study. The motivation for the authors was to use a commercially feasible and scalable approach to modifying surfaces towards reducing friction. In an industrial setting, surface grinding is well established in the machine tool industry and would need minimal investments, and it is commercially viable as compared to other surface modifying processes like laser surface texturing, plasma, or ion beam milling. Cao et al. [25] used cylindrical grinding as an effective way of creating defined textural patterns that help in reducing friction in a fully lubricated condition.

We used virgin sandpaper of P320, P800, P1200, and P2000 grit to create test specimens on mirror-finished stainless steel surfaces; 20 mL of water was sprayed using an atomizer bottle as the grinding lubricant, and the grinding time was controlled to 60 s. These machined specimens were tested for sliding friction on a pin-on-flat reciprocating tribometer for 1800 cycles; the reciprocating table was driven by a scotch yoke mechanism with a constant stroke length of 20 mm. A schematic of the tribometer and the loading arrangement is shown in Figure 2 below.

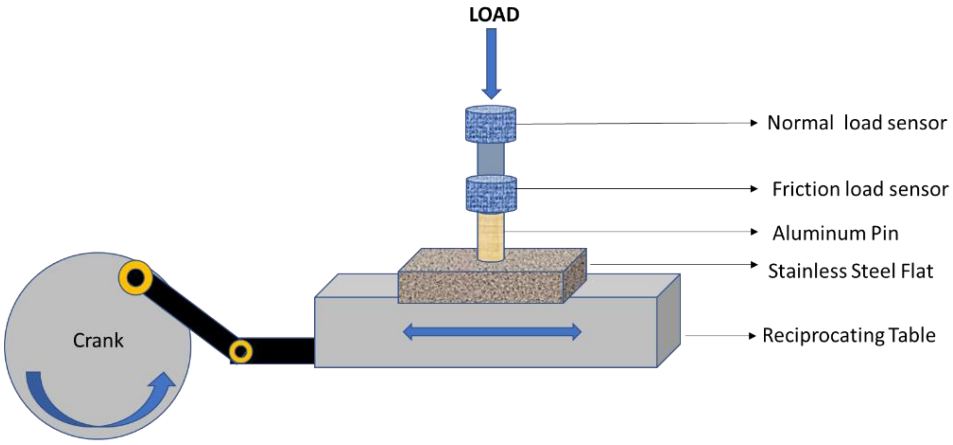

Figure 2. *Cont.*

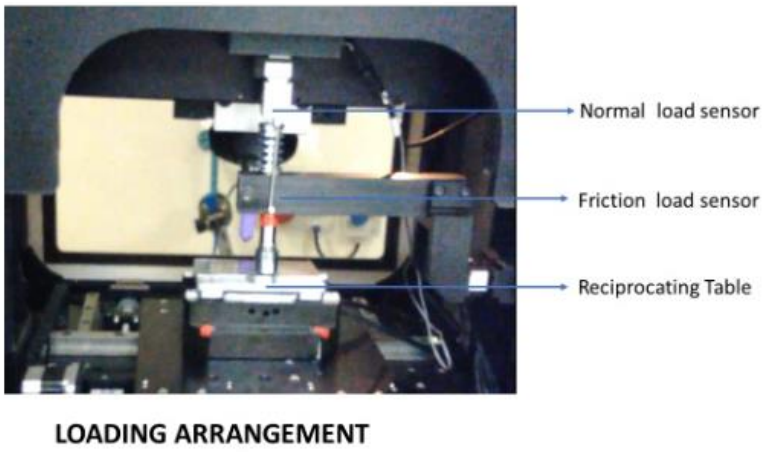

Figure 2. Schematic of the tribometer and the loading arrangement.

The velocity profile of the reciprocating table was sinusoidal as it was driven by a scotch yoke mechanism. Aluminum pins (6061 T6, Rockwell hardness B61) of 3 mm diameter were used in the test; pins were sourced from a single bulk stock. The pins were run-in before starting the test to ensure a flat-on-flat contact during sliding. To protect the surface texture of the flat specimens prepared while the aluminum pins were run-in, a polishing film of P5000 grade was secured over it. The importance of carefully controlling the pin surface during running-in was amply demonstrated by Hansen et al. [26]. The areal surface roughness was measured using a vertical scanning interferometer with an objective magnification of 10×. The normal load applied on the pins was 50 N, and the frequency of sliding was selected between 0.3 and 5 Hz over 1800 reciprocating cycles with a 20 mm stroke length; the total sliding distance was 72 m. The lubricant used was virgin API Group 1 SN500 base oil with a viscosity of 100 cSt at 40 °C and SN 150 Group 1 base oil with a viscosity of 30 cSt at 40 °C. We used a scanning electron microscope in back-scattered mode to identify changes in surface composition and image the surface topography; we used an energy dispersive spectrometer to quantify the composition of the surface and tribolayers.

The frictional force "F_x" as per the classical Stribeck curve, during boundary and mixed regime of lubrication, has an inverse relationship with the sliding velocity at the contact zone. The X axis of the Stribeck curve is represented as the dimensionless Hersey Number, represented as "$\eta \cdot N/P$", where "η" is the viscosity of lubricant in Ns/m^2, N is the relative velocity in m/s, and P is the load (newtons) per unit area. When this dimensionless number increases, the regime of lubrication shifts to the right. As the relative velocity designated by "N" increases, the film thickness of the lubricant film in the contact zone also increases [18], moving the lubrication regime to the right of the Stribeck curve.

Hence, in the boundary regime, the sliding velocity and the frictional force have an inverse relationship; the frictional force plot tends to a maximum at velocities approaching zero and tends to a minimum at increasing velocities during reciprocation. This is represented graphically in Figure 3 below where the velocity profile of the reciprocating table and the instantaneous frictional force along the stroke length is represented. Where the lubrication regime is assumed to be in the boundary and mixed region, the alternating "M" and inverted "M" patterns for frictional force seen below conform to the classical Stribeck behavior.

The test parameters for this study were chosen to ensure that the test regime operates to the left of the Stribeck curve where the boundary and mixed lubrication zones operate. The instantaneous friction occurring at the contact zone was continuously recorded at a data sampling rate of 100 Hz.

On this setup, our tests determining the average sliding coefficient of friction at 1 Hz for the different finished surfaces showed that the P1200 finished surface had the lowest sliding friction over other smoother and coarser surfaces. Since a reciprocating cycle consisted of alternating accelerating and decelerating domains apart from direction reversals, it was necessary to understand how the friction behaved in these domains, and

how the instantaneous frictional force changed along the sliding path in the stroke. We observed the contacts at different sliding frequencies of 0.3, 1, 2, and 5 Hz and different oil viscosities viz. SN 500 and SN 150 Group 1 base oils had a nominal viscosity of 100 cSt and 30 cSt at 40 °C, respectively. To tabulate and analyze the sliding friction response, we used the signals from the force sensor and averaged them over a sliding distance of 72 m, which meant 1800 reciprocating cycles for a 20 mm stroke length. This duration gave the authors sufficient time to observe the tribo-system while in the steady state regime.

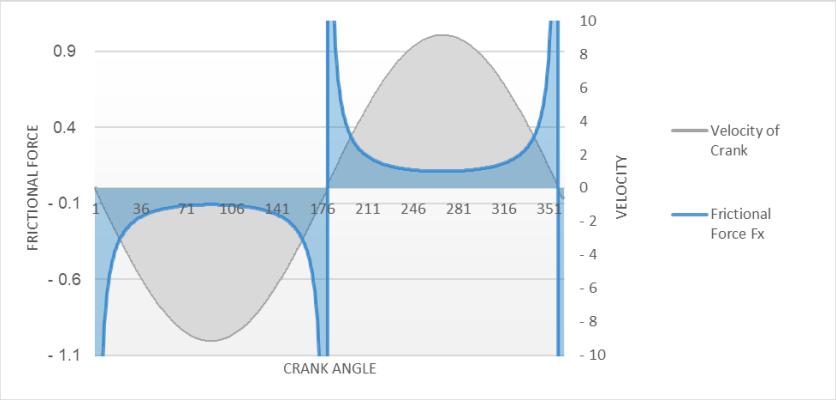

Figure 3. Velocity profile of the reciprocating table and the theoretical frictional force profile.

3. Results

The reciprocating table shown in Figure 2 had a scotch yoke drive; the instantaneous position and velocity of the table were dependent on the crank angle. The reciprocating table had a sinusoidal velocity profile; by plotting the instantaneous frictional force obtained along the location of the pin during sliding, we could get a peek into the mechanism of friction occurring at the contact interface.

In Figure 4, we plotted the average sliding coefficient of friction for our specimens. Using a normal load of 50 newtons, the applied contact pressure was 7.1 MPa. Representative specimens, viz. mirror, P1200, and P320 finished surfaces, were analyzed by logging the frictional force continuously over the sweep of the table through the stroke.

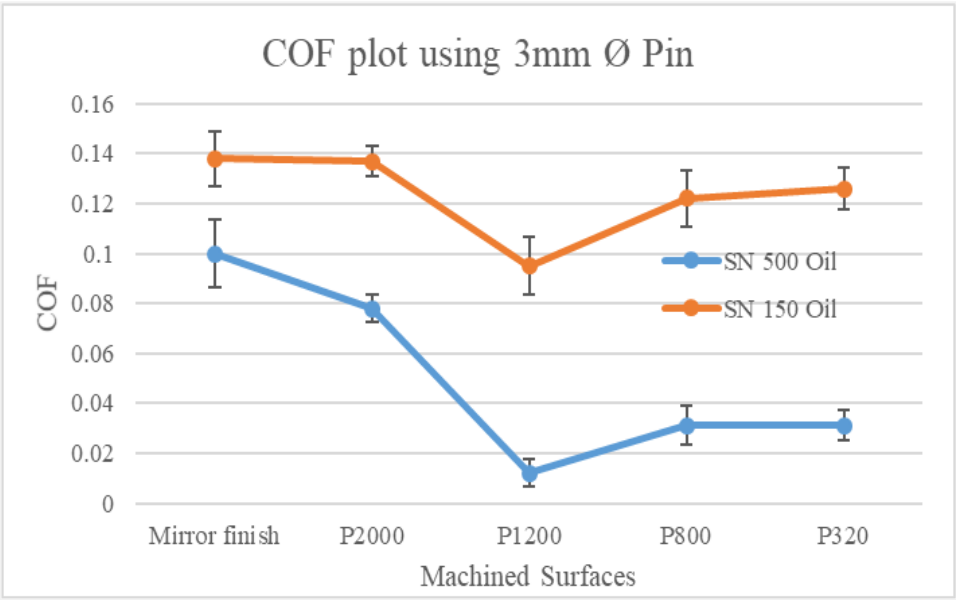

Figure 4. Cycle average COF for different topographies using a 3 mm diameter pin. The P1200 finished surface shows the lowest coefficient of friction.

The areal surface roughness parameters of our specimens were analyzed using vertical scanning interferometry and tabulated in Table 1 below.

Table 1. Mirror, P1200, and P320 finished surface scans using an optical interferometer.

Average Values of Areal Surface Roughness Parameters (in Microns)						
Surface Parameter	**Sa**	**Sku**	**Ssk**	**St**	**Sz**	**Sq**
P320	0.17	11.86	−1.90	5.70	4.62	0.24
P1200	0.04	19.60	−1.80	1.85	1.79	0.10
Mirror	0.02	1.8	−33.7	0.0053	0.0042	0.01

Gaussian filter applied with a S-Filter Cutoff of 8 µm and a L-Filter cutoff of 0.25 mm, Objective used was 10×.

Figure 5 shows the instantaneous frictional force on the pin during sliding for the three representative surfaces; the motion of the reciprocating table follows a sinusoidal velocity profile as was discussed in Section 3. The frictional forces were recorded at each position along the stroke and were averaged over 1800 cycles, which was the duration of the test. The thinner of the two oils, SN150, was used for sliding at 1 Hz reciprocating frequency.

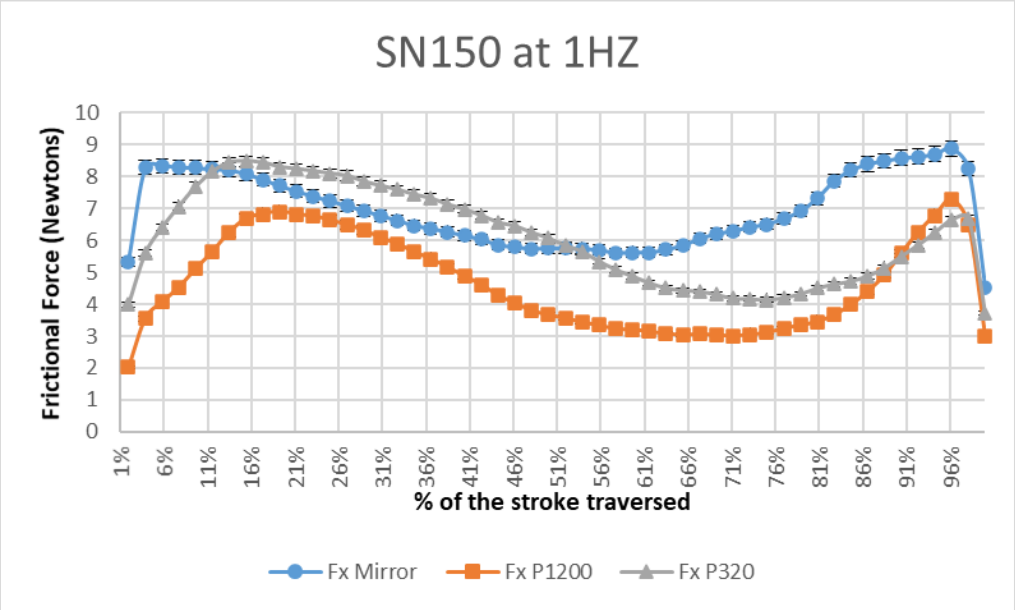

Figure 5. Average frictional force plot at 1 Hz for the different surfaces using SN 150 oil.

The shape of the frictional force plots on all three surfaces showed the broad 'M' and inverted 'M' shapes; we discussed the ideal shape of friction force curves following Stribeck behavior in Section 2, and these tribo-systems seem to be in close agreement.

Figure 6 shows the instantaneous frictional force on the pin during sliding, using the thicker SN500 oil. The viscosity of this base oil is about three times higher than the SN150 oil used in the previous test.

The samples were now tested at other sliding frequencies of 0.3, 2, and 5 Hz, and the corresponding frictional plots were compared for the three surfaces. The peak and average sliding velocities corresponding to the different frequencies are listed in Table 2; the peak velocities occurred in the middle of the stroke.

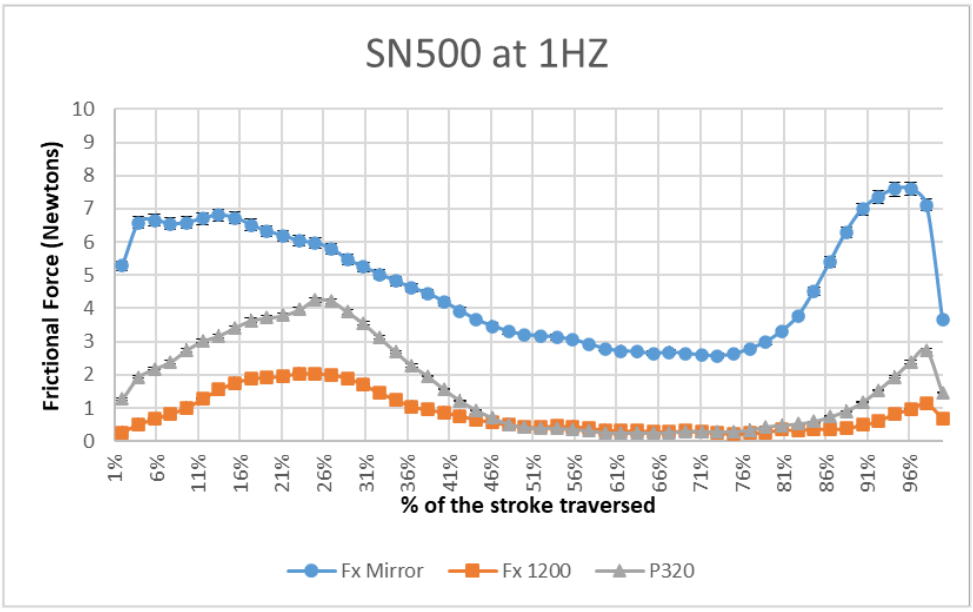

Figure 6. Average frictional force plot at 1 Hz for the different surfaces using SN 500 oil.

Table 2. Average and peak velocities for different sliding frequencies of the pin-on-flat.

Stroke = 20 mm			
Sr No:	**Sliding Frequency (Hz)**	**Avg. Velocity (mm/s)**	**Peak Velocity (mm/s)**
1	0.3	12	37.7
2	1	40	125.7
3	2	80	251.4
4	5	200	628.6

Figure 7 shows the frictional plot on all three surfaces using a lower reciprocating frequency of 0.3 Hz.

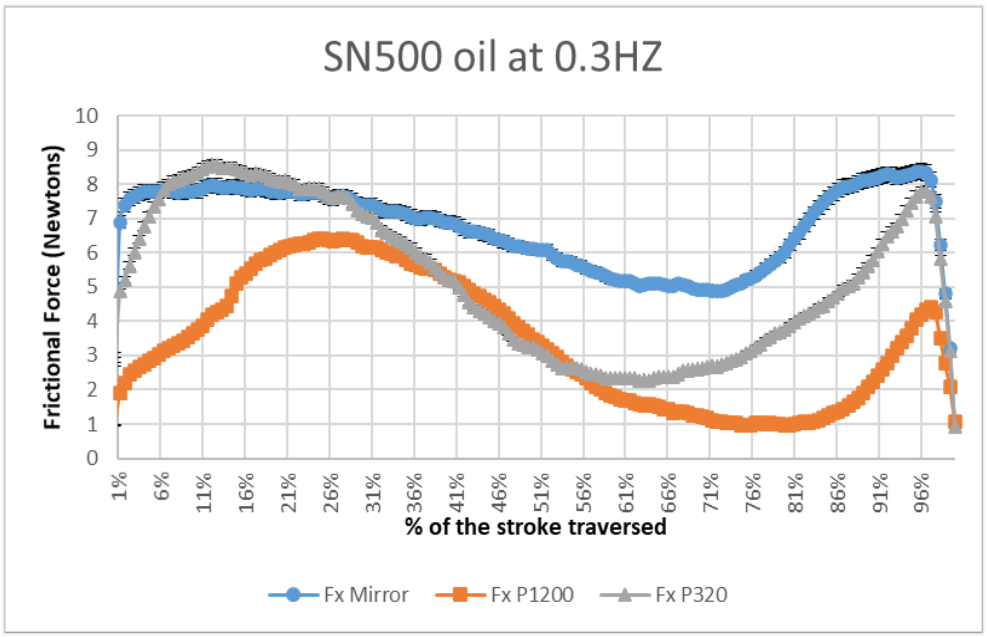

Figure 7. Average frictional force plot at 0.3 Hz for the different surfaces using SN 500 oil.

The magnitude of friction was higher than in Figure 6, where the test was conducted with SN500 oil and at 1 Hz. We could observe that all three surfaces showed the broad 'M' pattern we had earlier discussed for the force curves following Stribeck behavior. Figure 8 shows the frictional plot at a higher reciprocating frequency of 2 Hz. The magnitude of friction dropped below 1 N for most parts of the sliding for the P1200 and P320 surfaces. Figure 9 shows the frictional plot at our highest reciprocating frequency of 5 Hz. The magnitude of friction dropped below 0.5 N for most parts of the sliding on P1200 and P320 surfaces. While at 1 Hz and higher speeds, the oil was seen to be collecting ahead of the pin especially evident during deceleration, but this observation was not present at the lower reciprocating frequency of 0.3 Hz.

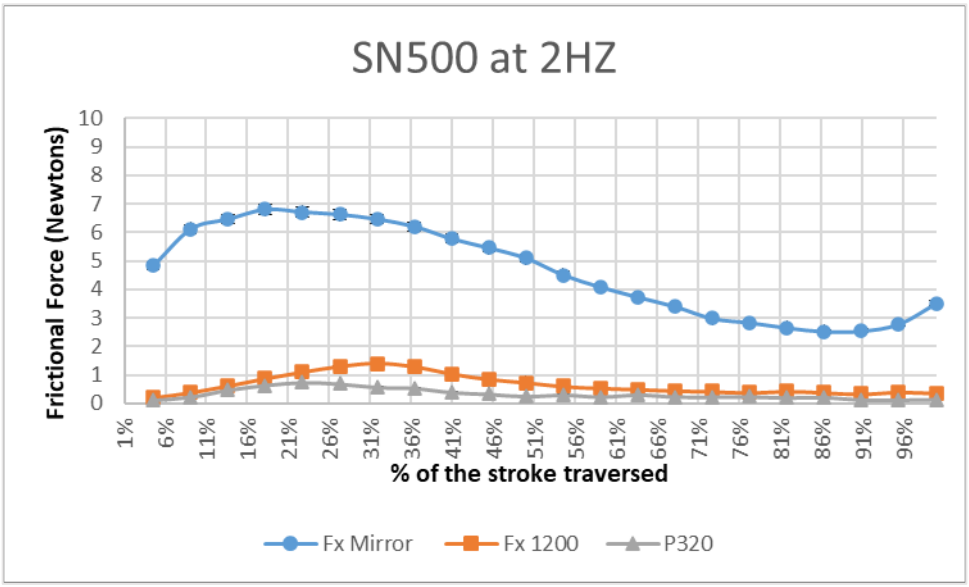

Figure 8. Average frictional force plot at 2 Hz for the different surfaces using SN 500 oil.

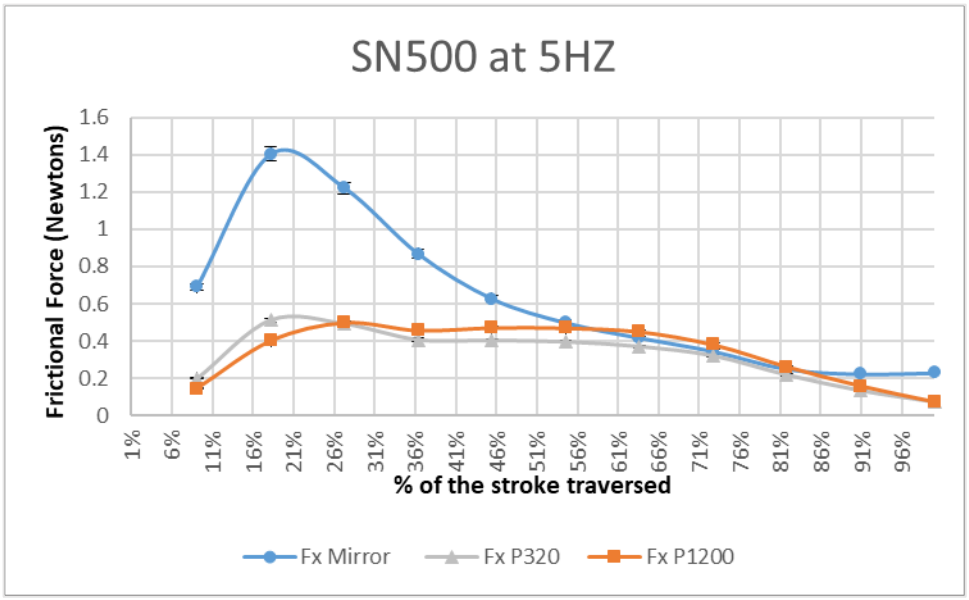

Figure 9. Average frictional force plot at 5 Hz for the different surfaces using SN 500 oil.

Surface images were captured using a scanning electron microscope after the test duration of 1800 cycles of sliding at 1 Hz on the mirror, P1200, and P320 finished surfaces, which are shown in Figures 10–12, respectively.

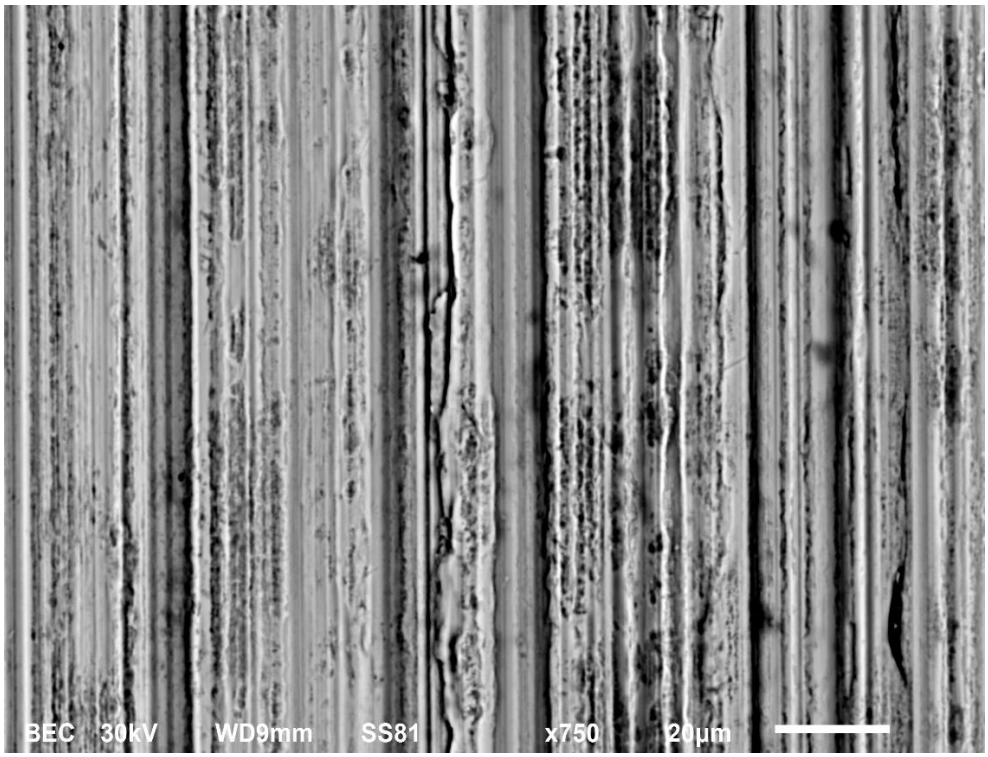

Figure 10. Back-scattered SEM image of the mirror surface after completion of the sliding test at 1 Hz. Heavy material movement along the direction of sliding involving adhesive sliding wear was observed.

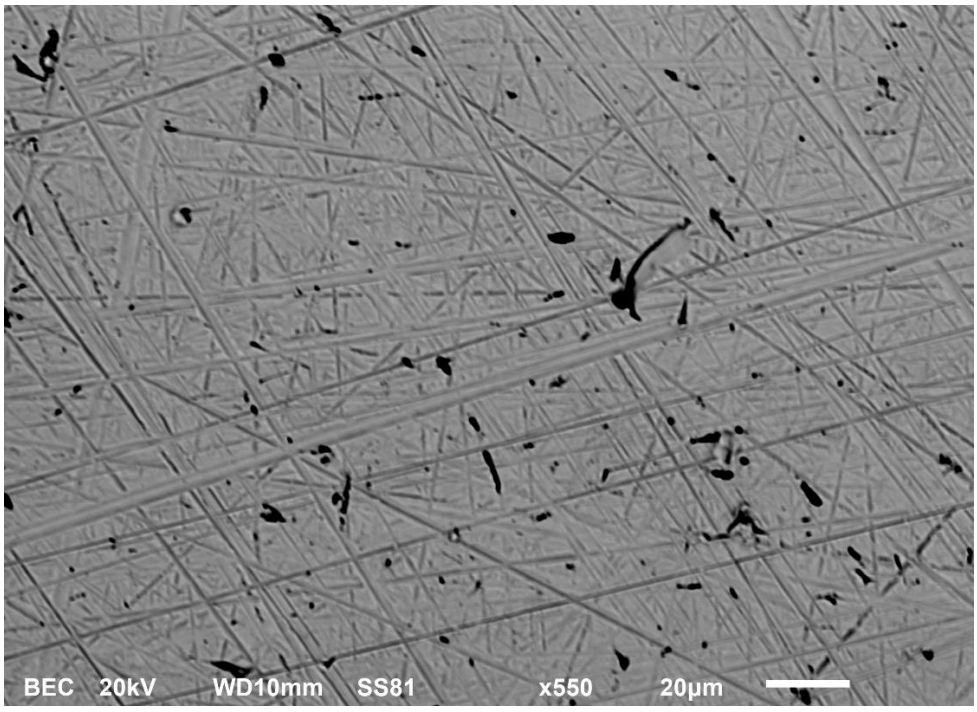

Figure 11. Back-scattered SEM image of the P1200 finished surface after completion of the sliding test at 1 Hz. The surface indicates minimal wear.

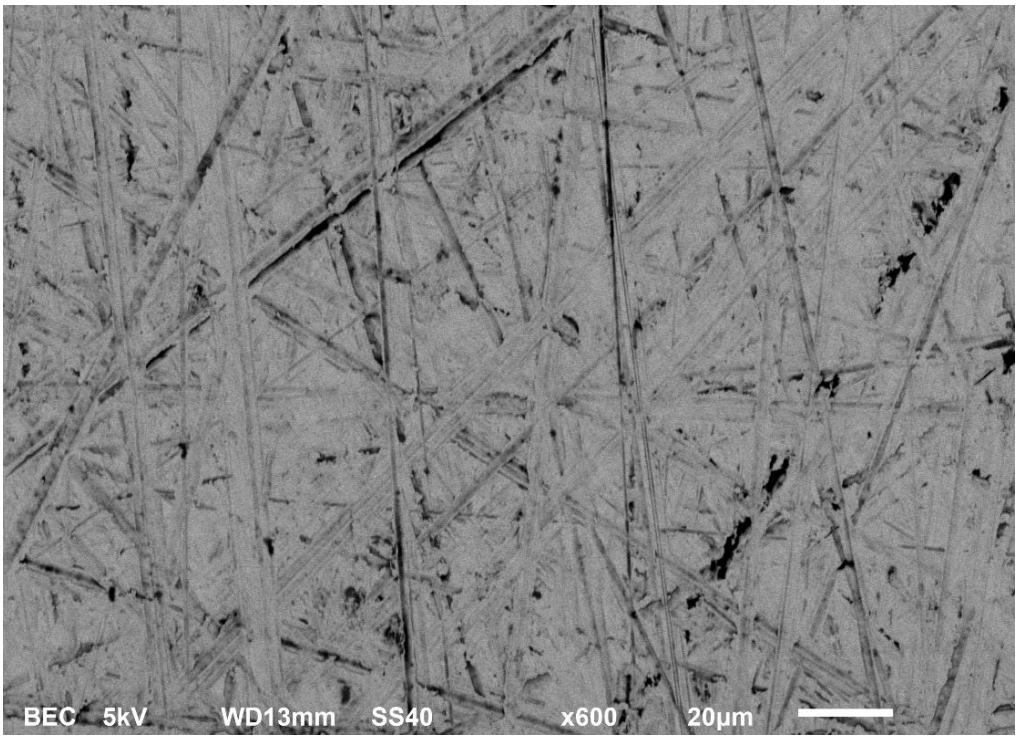

Figure 12. Back-scattered SEM image of the P320 finished surface after completion of the sliding test at 1 Hz. Abrasive scouring marks were observed on the surface.

The next series of tests were conducted with the SN 500 base oil doped with the ZDDP that helps forms the anti-wear tribofilm.

In Figure 13, the frictional force is plotted against the sliding time while using the ZDDP-doped oil for the mirror-finished surface. Figure 14 shows the P320 finished surface sliding with the ZDDP-doped oil. These plots were overlaid with the undoped force plots that were obtained in the previous tests.

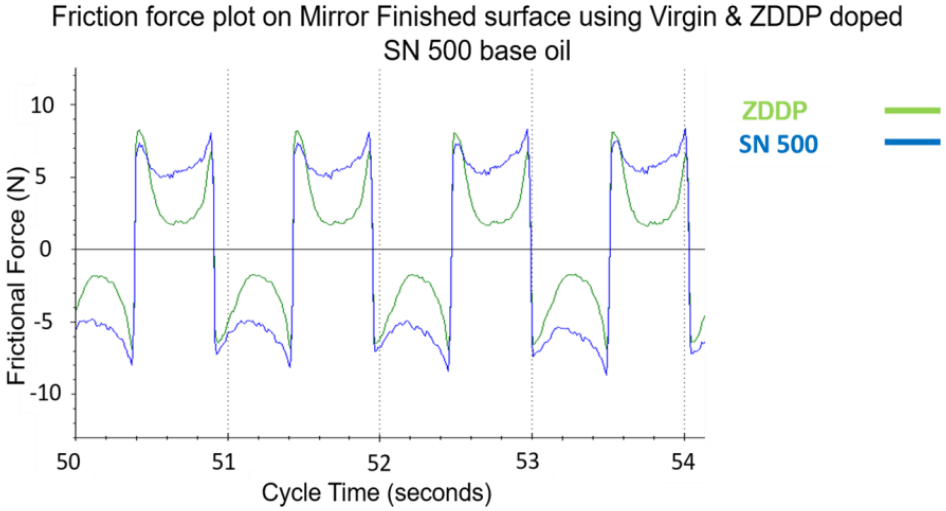

Figure 13. Friction force plot on the mirror-finished surface using virgin and ZDDP doped SN 500 base oil.

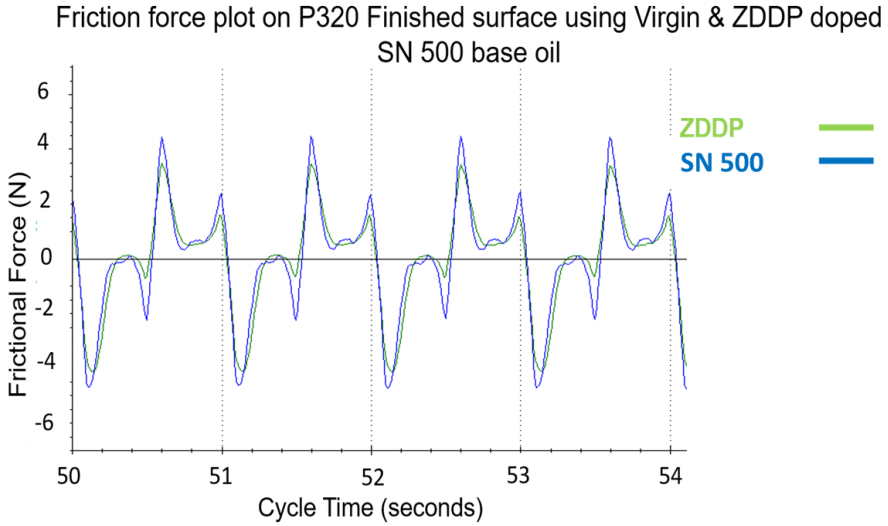

Figure 14. Friction force plot on P320 finished surface using virgin and ZDDP doped SN 500 base oil.

4. Discussion

We used the plot in Figure 3 to compare friction force profiles obtained in our sliding experiments. For the mirror, P1200, and P320 finished specimens, sliding tests were conducted with two different viscosities. While using the low-viscosity oil, the plot shape seen in Figure 5 resembled the 'M' pattern we plotted in Figure 3. Among the three surfaces showing this pattern, the P1200 had the lowest magnitude of sliding friction. The origin of the 'M' pattern for a reciprocating sliding system was discussed in Section 2; the above system closely matched the regimes of lubrication when the sliding contact accelerated and decelerated. With the higher oil viscosity seen in Figure 6, the 'M' pattern was still seen, albeit faintly. As the contact progressed towards the middle of the stroke, the friction force steadily decreased. For the P320 and P1200 surfaces, the plots almost seemed to touch the abscissa. Clearly, the magnitude of friction was lower on all the surfaces when compared to the previous test.

The P1200 surface showed a unique synergy with this viscosity by lowering the peak friction by more than 70% compared with the previous test. P1200 also had the lowest peak friction among the three surfaces, about 50% lower than P320 and 70% lower than the mirror-finished surface. This explains why the shape of the force plots departs from the 'M' pattern. With the ground surfaces, we noticed that the friction peak during deceleration was smaller than during acceleration. As the contact was decelerating, the leading edge of the pin was seen collecting a considerable amount of oil. Stahl et al. [27] investigated the influence of fluid volume on friction between rough surfaces with the aid of the Stribeck curve. While characterizing hydrodynamic, mixed, or boundary friction and its dependence, they observed that the fluid quantity had a deeper influence on the load regime than other parameters like velocity. With the surface roughness being an order of magnitude higher for the P1200 and P320 over the mirror specimens, the topography would have been responsible for retaining a higher quantity of the lubricant, aiding in lower friction during deceleration. On the mirror-finished samples, we could not observe this phenomenon happening until the frequency was increased to 2 Hz or higher as seen in Figures 8 and 9. Interestingly when the frequency was reduced to 0.3 Hz as seen in Figure 7, this phenomenon was still seen clearly on the P1200, while on the P320 finished surface, this was only faintly visible. The synergy of the P1200 surface with the higher viscosity oil was thus obvious at 0.3 and 1 Hz.

At the 0.3 Hz as seen in Figure 7, all three specimens had a similar shape of frictional response depicting the 'M' pattern. The shape of the frictional force plots was similar to that seen in Figure 5, where we used the low-viscosity oil for sliding at 1 Hz. Stribeck' s experiments [28] observed that when the bearing speed approached zero, all tested loads

gave the same coefficient of friction, and at low speeds, an increase in the metal-to-metal contact led to an increase in the oil temperature. The lowest friction was still seen for the P1200 surface. The accumulation of oil at the leading edge of the pin was observed to be a lot lower than at 1 Hz, as was evident from the friction curve shapes during the decelerating phase.

When the reciprocating frequency was increased to 2 Hz as seen in Figure 8, the P320 and the P1200 surfaces had nearly overlapping plots, with the P1200 surface having about a 1 N higher magnitude of the peak frictional force. The lowest friction on all surfaces was evident in the decelerating regime just beyond 80% of the stroke traversal. The friction peak on the mirror surface was nearly 70% higher than on the ground surfaces.

At a still higher frequency of 5 Hz as seen in Figure 9, the frictional forces were an order of magnitude lower than the previous tests. During the decelerating domain, we observed that the topographies became irrelevant as the force plots overlapped and tended to 0.2 N, which was the lowest magnitude of frictional force seen in all our sliding tests. Higher sliding speeds meant higher film thickness at the contact zone, where the broad differences in friction between rough and smooth surfaces vanished; this was noted by Guegan et al. [29], Bayer [17], and Hutchings [30]. Here again, the lowest friction was seen in the decelerating domain and beyond 90% of the stroke traversal. From the above, it seemed that with the increasing speed of reciprocation, the minimum friction point was shifting to the right side of the friction force plot, pointing to the increasing oil volume swept ahead of the pin before the pin velocity reached zero. It can be argued that owing to the inertia of the oil film collected ahead of the pin, a faster speed of reciprocation meant a greater quantity of oil collected ahead of the pin and at the pin flat interface. This enabled the tribo-system to shift to the right of the Stribeck curve to operate in the hydrodynamic regime for a longer part of the cycle. The maximum friction was seen for the mirror surface at 1.4 N during the accelerating domain where the COF was only 0.028. From the mid-point of the stroke, the friction reduced drastically, and the rest of the plot was very similar to the ground surfaces. The P320 surface showed about a 0.5 N lower magnitude of friction than the P1200 surface; this behavior was also seen in Figure 8 at the reciprocating frequency of 2 Hz. At higher speeds where a full film lubrication regime exists, the rougher topography of the P320 could have been responsible for a microscopic hydrodynamic action giving it slightly lower friction. Masuko et al. [31] and Borras et al. [32] discussed the microscopic hydrodynamic action in their experiments, wherein the rougher surfaces in sliding could record slightly lower friction.

To discuss the surface phenomena happening at 1 Hz in greater detail, the frictional force curve was extracted for the last reciprocating cycle and overlaid in Figure 15. The P1200 surface displayed the lowest frictional force at 1 N, which corresponds to a COF of 0.02. The shapes of the plots were distinctly different from each other; this comes from the contribution of topography brought in by the ground surfaces. Surface topography images of the mirror-finished surface after sliding in Figure 10 showed significant surface delamination and material shifting along the direction of sliding, suggesting high adhesive wear. On a comparatively rougher specimen like the P320 surface, the topography image in Figure 12 did not suggest any material delamination brought in by adhesive wear; however, ploughing and scouring marks could be seen, which were brought about by the abrasive wear removal during the linear sliding motion. After sliding, the P1200 surface displayed a topography with minimal wear, as seen in Figure 11. The P1200 specimens featured only random scratch marks, which were generated from the sample grinding stage on the rotary polisher; however, no perceivable wear marks could be seen in the direction of sliding as was seen for the other surfaces.

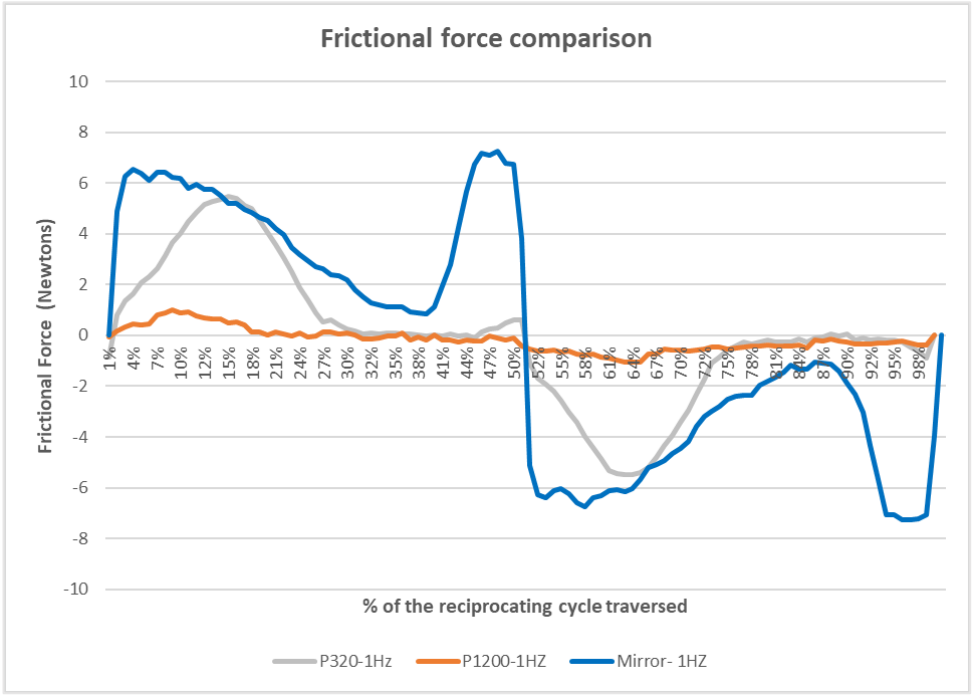

Figure 15. Friction force plot overlaid for different surfaces at 1 Hz using SN500 oil.

Since adhesive wear dominated during the sliding of the mirror-finished surface, we further observed the frictional force plots after doping our test oil with a tribofilm-forming additive that limits the adhesive wear mechanism. A primary alkyl, zinc di-alkyl di-thiophosphate (ZDDP), of a molecular weight of 716.38, having 9% by weight of zinc and 8% by weight of phosphorous, was used for this test. Zhang et al. [33] noted that ZDDP protects the mating surfaces from adhesive wear by reacting with the parent steel surface to form a sacrificial tribolayer; this was triggered by localized heating and pressure build-up at the contact zone. In Figure 13, the frictional force is plotted against the sliding interval and overlaid with the doped and undoped oil. After doping, the sliding friction drops to the minimum at the middle of the stroke where the sliding velocity is the maximum and increases as the velocity decreases until the direction reversal happens. Comparing it with the undoped oil, the friction is seen to be high at the middle of the stroke, indicating adhesion. On the P320 finished surface, as seen in Figure 14, there is no visible effect of the introduction of the tribofilm on the sliding friction. This observation supports the hypothesis that adhesive friction was dominant during sliding on the mirror-finished specimens and relatively insignificant during sliding on a rougher surface like the P320.

The shape of the frictional force plots obtained in our experiments with different sliding velocities and oil viscosities suggest the presence of a threshold frequency of reciprocation, below which the shape of these plots followed the shape of the Stribeck curve. This threshold is seen to be independent of the topography. Table 3 shows a summary of the frictional response for different sliding interfaces formed by a combination of different topographies and sliding velocities.

There seems to be a fine balance that needs to be achieved between adhesion and abrasion versus oil retention while demonstrating extremely low sliding friction. Asperities promote abrasive wear. Flat surfaces promote adhesive wear. A compromise in asperity height achieves low adhesion and oil retention while not enhancing the abrasion. Polished and finished surfaces have too much adhesion. P320 finished surfaces have too many abrasion effects, even though their roughness will promote more oil retention.

Table 3. Summary of sliding frictional response for different topographies and sliding velocities." √" represents YES and "X "represents NO.

Sliding Frictional Response	**Topography by**		
Frictional Response at 0.3 HZ using SN500 Oil	None (Mirror)	P1200	P320
Follows Perfect Stribeck Behavior, Alternating "M" and "W" Patterns	√	√	√
Acceleration response present, decelaration absent	X	X	X
Frictional Response extremely low	X	X	X
Frictional Response at 1 HZ using SN500 Oil	Mirror	P1200	P320
Follows Perfect Stribeck Behavior, Alternating "M" and "W" Patterns	√	X	X
Acceleration response present, decelaration absent	X	X	√
Frictional Response extremely low	X	√	X
Frictional Response at 2 HZ using SN500 Oil	Mirror	P1200	P320
Follows Perfect Stribeck Behavior, Alternating "M" and "W" Patterns	√	X	X
Acceleration response present, decelaration absent	X	X	X
Frictional Response extremely low	X	√	√
Frictional Response at 5 HZ using SN500 Oil	Mirror	P1200	P320
Follows Perfect Stribeck Behavior, Alternating "M" and "W" Patterns	X	X	X
Acceleration response present, decelaration absent	X	X	X
Frictional Response extremely low	√	√	√

5. Conclusions

Mirror-finished stainless steel surfaces were machined with different commercially available coated abrasives of grits P2000, P1200, P800, and P320 using a laboratory-scale rotary table grinder. One of these surfaces showed an extraordinary reduction in the average coefficient of sliding friction when tested against a reciprocating aluminum flat-faced pin. It was noted that the average surface roughness of these surfaces did not differ very much from each other. We believe that surface grinding towards achieving a specific topography that synergizes well with the application and the lubricant applied helps towards reducing friction in a cost-effective and scalable manner.

Plotting sliding friction in real-time helped analyze how the friction behaved when the contacts were accelerating, reaching the peak velocity of sliding and decelerating approaching the end of the stroke before reversing the direction of sliding. Comparing the height of friction force peaks during acceleration and deceleration provided insights into the quantum of oil retention induced by different surfaces after grinding. The shapes of the frictional curves could help understand when the tribo-system and surface parameters were approaching conditions for generating the Stribeck curve.

The ability of surface topography to reduce friction by the mechanism of retaining lubricant appears to be the primary mechanism when the lubricant availability is limited at the contact zone. When the oil viscosity and the sliding speed were increased, they seemed

to support the retention of the oil film in the reciprocating domain, and the lubrication regime for ground surfaces shifted from the boundary to the right of the Stribeck curve. When sliding experiments were performed under contact pressure not exceeding 7.5 MPa, the stainless steel flat ground using a P1200 coated abrasive showed the lowest average coefficient of friction of 0.02 while using an SN500 base oil. The synergistic combination of surface topography, oil viscosity, and sliding velocity can allow the oil to support the load, leading to extremely low values of sliding friction; this can be applied to practical engineering applications to reduce the useful energy otherwise lost in overcoming friction.

Author Contributions: Conceptualization, G.P., V.J. and S.V.K.; methodology, G.P.; formal analysis, G.P., V.J. and S.V.K.; investigation, G.P.; resources, V.J. and S.V.K.; data curation, G.P.; writing—original draft preparation, G.P.; writing—review and editing, V.J. and S.V.K. All authors have read and agreed to the published version of the manuscript.

Funding: This research received no external funding.

Data Availability Statement: All relevant data are presented in the paper.

Acknowledgments: We thank the staff and students of the Department of Materials Engineering and the Department of Mechanical Engineering, Indian Institute of Science, Bangalore, for all the administrative and technical support given to us for performing our work. We also thank S.K. Biswas (Late) under whose vision we could start our work and crystallize our thought process.

Conflicts of Interest: The authors declare no conflict of interest.

Abbreviations

The SN 150	Group 1 solvent neutral lubricant base oil having an ISO viscosity grade of 30 cSt at 40 °C.
SN 500	Group 1 solvent neutral lubricant base oil having an ISO viscosity grade of 100 cSt at 40 °C.
Fx	Frictional force.
P2000, P1200, P320	PSA liner paper backed coated abrasives as per FEPA (P- Scale) based on mean grain size of abrasive mineral ds 50 particle size.
Hz	Unit of reciprocating frequency expressed as Hertz.
MPa	S.I. unit of pressure abbreviated as mega Pascals.
ZDDP	Zinc di-alkyl di-thio phosphate.
µm	An SI derived unit of length equaling 1×10^{-6} m and expressed as micrometer.
S-filter	A filter eliminating the smallest scale elements from the surface (low-pass filter) during a surface roughness measurement.
L-Filer	A filter eliminating the largest scale elements from the surface (high-pass filter) during a surface roughness measurement.

References

1. Nosonovsky, M. Oil as a Lubricant in the Ancient Middle East. *Tribol. Online* **2007**, *2*, 44–49. [CrossRef]
2. Shillito, L. Building Stonehenge? An alternative interpretation of lipid residues in Neolithic Grooved Ware from Durrington Walls. *Antiquity* **2019**, *93*, 1052–1060. [CrossRef]
3. Barthlott, W.; Neinhuis, C. Purity of the sacred Lotus, or Escape from Contamination in Biological Surfaces. *Planta* **1997**, *202*, 1–8. [CrossRef]
4. Neinhuis, C.; Barthlott, W. Characterization and Distribution of Water-Repellent, Self-Cleaning Plant Surfaces. *Ann. Bot.* **1997**, *79*, 667. [CrossRef]
5. Sun, G.; Fang, Y.; Cong, Q.; Ren, L.-Q. Anisotropism of the Non-Smooth Surface of Butterfly Wing. *J. Bionic Eng.* **2009**, *6*, 71–76. [CrossRef]
6. Yamamoto, M.; Nishikawa, N.; Mayama, H.; Nonomura, Y.; Yokojima, S.; Nakamura, S.; Uchida, K. Theoretical Explanation of the Lotus Effect: Superhydrophobic Property Changes by Removal of Nanostructures from the Surface of a Lotus Leaf. *Langmuir* **2015**, *31*, 7355–7363. [CrossRef]
7. Evans, C.J.; Bryan, J.B. "Structured", "textured" or "engineered" surfaces. *CIRP Ann. Manuf. Technol.* **1999**, *48*, 541–556. [CrossRef]
8. Stout, K.J.; Spedding, T.A. The characterization of internal combustion engine bores. *Wear* **1982**, *83*, 311–326. [CrossRef]
9. Kligerman-Ryk, G.; Kligerman, Y.; Etsion, I. Experimental investigation of laser surface texturing for reciprocating automotive components. *Tribol. Trans.* **2002**, *45*, 444–449.

10. Kovalchenko, A.; Ajayi, O.; Erdemir, A.; Fenske, G.; Etsion, I. The effect of laser surface texturing on transitions in lubrication regimes during unidirectional sliding contact. *Tribol. Int.* **2005**, *38*, 219–225. [CrossRef]
11. Etsion, I.; Kligerman, Y.; Halperin, G. Analytical and experimental investigation of laser-textured mechanical seal faces. *Tribol. Trans.* **1999**, *42*, 511–516. [CrossRef]
12. Etsion, I.; Halpmaerin, G. A laser surface textured hydrostatic mechanical seal. *Tribol. Trans.* **2002**, *45*, 430–434. [CrossRef]
13. Ronen, A.; Etsion, I.; Kligerman, Y. Friction-reducing surface texturing in reciprocating automotive components. *Tribol. Trans.* **2001**, *44*, 359–366. [CrossRef]
14. Willis, E. Surface Finish in Relation to Cylinder Liners. *Wear* **1986**, *109*, 351–366. [CrossRef]
15. Schnell, G.; Müller, T.; Seitz, H. Tribological effects of different scaled chevron-shaped microstructures on the Stribeck curve of parallel contacts under unidirectional friction. *Tribol. Int.* **2023**, *178*, 108099. [CrossRef]
16. Erdemir, A. Review of engineered tribological interfaces for improved boundary lubrication. *Trib. Int.* **2005**, *38*, 249–256. [CrossRef]
17. Bayer, R.G. *Mechanical Wear Prediction and Prevention*; Marcel Dekker Inc.: New York, NY, USA, 1994.
18. Ludema, K.C. *Friction, Wear, Lubrication: A Textbook in Tribology*; CRC Press: Boca Raton, FL, USA, 1996; 257p.
19. Pettersson, U.; Jacobson, S. Textured surfaces in sliding boundary lubricated contacts—Mechanisms, possibilities and limitations. *Tribol.-Mater. Surf. Interfaces* **2007**, *1*, 181–189. [CrossRef]
20. Pettersson, U.; Jacobson, S. Influence of surface texture on boundary lubricated sliding contacts. *Tribol. Int.* **2003**, *36*, 857–864. [CrossRef]
21. Menezes, P.L.; Kailas, S.V. Effect of surface roughness parameters and surface texture on friction and transfer layer formation in tin-steel tribo-system. *J. Mater. Process. Technol.* **2008**, *208*, 372–382. [CrossRef]
22. Menezes, P.L.; Kishore; Kailas, S.V. Studies on friction and transfer layer: Role of surface texture. *Tribol. Lett.* **2006**, *24*, 265–273. [CrossRef]
23. Wang, Z.; Zhao, Q.; Wang, C. Reduction of Friction of Metals using Laser Induced Periodic Surface Nanostructures. *Micromachines* **2015**, *6*, 1606–1616. [CrossRef]
24. Maru, M.M.; Trommer, R.M.; Cavalcanti, K.F.; Figueiredo, E.S.; Silva, R.F.; Achete, C.A. The Stribeck curve as a suitable characterization method of the lubricity of biodiesel and diesel blends. *Energy* **2014**, *69*, 673–681. [CrossRef]
25. Cao, H.; Chen, X.; Li, H.; Shen, C. Frictional Behaviour of the Microstructural Surfaces Created by Cylindrical Grinding Processes. *Appl. Sci.* **2022**, *12*, 618. [CrossRef]
26. Hansen, E.; Frohnapfel, B.; Codrignani, A. Sensitivity of the Stribeck curve to the pin geometry of a pin-on-disc tribometer. *Tribol. Int.* **2020**, *151*, 106488. [CrossRef]
27. Stahl, L.; Müller, M.; Ostermeyer, G.P. On the experimental characterization of the fluid volume influence on the friction between rough surfaces. *Friction* **2023**, *11*, 1334–1348. [CrossRef]
28. Jacobson, B. The Stribeck Memorial Lecture. *Tribol. Int.* **2003**, *36*, 781–789. [CrossRef]
29. Guegan, J.; Kadiric, A.; Gabelli, A.; Spikes, H. The Relationship Between Friction and Film Thickness in EHD Point Contacts in the Presence of Longitudinal Roughness. *Tribol. Lett.* **2016**, *64*, 33. [CrossRef]
30. Hutchings, I.M. *Tribology: Friction and Wear of Engineering Materials*; Edward Arnold: Oxford, UK, 1992; p. 273.
31. Masuko, M.; Aoki, S.; Suzuki, A. Influence of Lubricant Additive and Surface Texture on the Sliding Friction Characteristics of Steel under Varying Speeds Ranging from Ultralow to Moderate. *Tribol. Trans.* **2005**, *48*, 289–298. [CrossRef]
32. Borras, F.X.; de Rooij, M.B.; Schipper, D.J. Misalignment-Induced Micro-Elastohydrodynamic Lubrication in Rotary Lip Seals. *Lubricants* **2020**, *8*, 19. [CrossRef]
33. Zhang, J.; Spikes, H. On the Mechanism of ZDDP Antiwear Film Formation. *Tribol. Lett.* **2016**, *63*, 24. [CrossRef]